Catalysis Science & Technology

Accepted Manuscript

ROYAL SOCIETY OF CHEMISTRY

www.rsc.org/catalysis

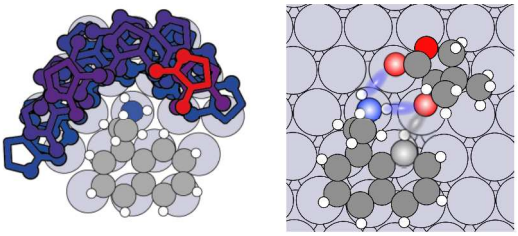

Revealing the set of most stable bimolecular complexes formed by a prochiral molecule and a chiral modifier on Pt(111)

Single-Chiral-Catalytic-Surface-Sites: STM and DFT Study of Stereodirecting Complexes Formed Between (*R*)-1-(1-naphthyl)ethylamine and Ketopantolactone on Pt(111)

Katrine Svane[1], Yi Dong[2], Michael N. Groves[1], Vincent Demers-Carpentier[2], Jean-Christian Lemay[2], Mireille Ouellet[2], Bjørk Hammer[1], and Peter H. McBreen[2]

[1]iNano and Department of Physics and Astronomy, Aarhus University, 8000 Aarhus C, Denmark
[2]Department of Chemistry, Laval University, Quebec City, Quebec, G1K 7P4, Canada

E-mail: hammer@phys.au.dk; peter.mcbreen@chm.ulaval.ca

Abstract

The formation of bimolecular complexes on metal surfaces through interaction between a single chemisorbed chiral molecule and a single chemisorbed prochiral substrate molecule can be considered as a preorganization step toward chirality transfer. In the case of asymmetric hydrogenation on chirally modified platinum catalysts, the metal surface dissociates H_2 and provides atomic hydrogen for the desymmetrization step. Along the reaction path, the combined chemisorption and intermolecular interactions in the assembly formed between the modifier and the substrate determine which enantiomer is formed in excess. In this study, we use DFT calculations and STM measurements to describe chemisorption and intermolecular interactions in isolable structures formed between single ketopantolactone and single (*R*)-1-(1-naphthyl)ethylamine molecules on Pt(111). The study reveals several distinct complexation geometries at the sub-molecular level as well as the stereodirecting forces operating in the most abundant bimolecular assemblies. The comparison of theoretical and experimental data strongly suggests that partial hydrogenation of KPL occurs under the experimental conditions and that some of the most abundant complexes are formed by the hydroxy intermediate.

Introduction

The chemisorption of chiral molecules on metals can be used to create catalytic sites that are active for asymmetric synthesis reactions.[1-7] This so-called chiral modifier approach is exploited in the enantioselective hydrogenation of activated ketones on supported Pt particles.[1] In terms of enantioselectivity and substrate scope, cinchona alkaloids, such as cinchonidine, are the best performing chiral modifiers for this reaction, as first reported by Orito et al.[8] However, the simpler synthetic modifier, 1-(1-naphthyl)ethylamine, (NEA), has also been shown to be effective.[9,10] For example,

Baiker and co-workers[9] used (*R*)-NEA on Pt/Al_2O_3 to effect the asymmetric hydrogenation of ketopantolactone (KPL) to (*R*)-pantolactone (Fig. 1) with an enantiomeric excess (*ee*) of 52%.

Stereochemical bias in such chirally modified metal catalyst systems is believed to arise through chemisorption and complexation of the substrate in the asymmetric surface environment created by the modifier. That is, the substrate is forced by the combined action of the modifier and metal to preferentially turn one enantiotopic face towards the metal surface. Under purely thermodynamic control, and ignoring hydrogenation on achiral regions of the surface, the resulting prochiral ratio in complexes (pro-R:pro-S) is expected to determine the enantiomeric ratio (*R*:*S*) of the product.[1] Under kinetic control, the relative rates of hydrogenation in pro-R and pro-S complexes will dictate the outcome (again, ignoring competing racemic hydrogenation on achiral regions of the surface).[1] Hence, in relation to the KPL/(*R*)-NEA/Pt system, where the enantiomeric ratio (76:24, Figure 1) is known from catalysis measurements,[9] it is interesting to use surface science techniques to probe the pro-R:pro-S ratio in KPL/(*R*)-NEA complexes on the surface of a Pt single crystal. Such measurements provide a means to explore if there is a relationship between the preorganization structure of modifier-substrate complexes formed on metal surfaces and the enantiomeric ratio observed in the corresponding catalytic reaction.

Here, we use a combination of scanning tunneling microscopy (STM) and density functional theory (DFT) to probe the chemisorption structure and intermolecular interactions in modifier-substrate complexes formed between (*R*)-NEA and KPL on Pt(111). The chemisorption of NEA has also been studied by other groups in relation to the Orito reaction.[11,12] The (111) face of Pt is particularly well suited for our model study as shown by shape-selective Pt nanoparticle studies by Baiker and co-workers.[13] While the model study will not capture the full complexity of processes occurring in solution, it is likely to provide general insight on stereodirection at single chiral sites, and in that way advance an overall understanding of heterogeneous asymmetric catalysis.

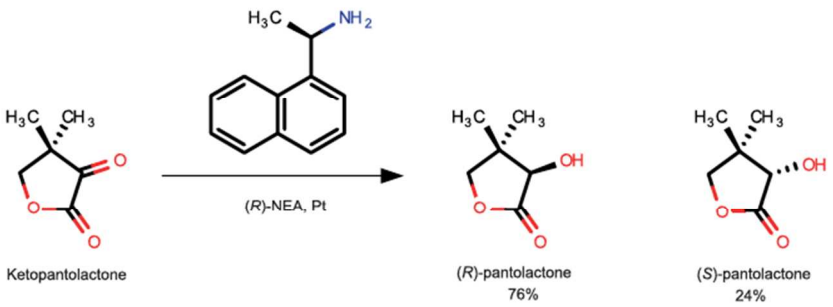

Figure 1. Asymmetric hydrogenation of ketopantolactone (KPL) on (*R*)-NEA modified Pt/Al_2O_3 in acetic acid.[9]

In previous work, we combined STM and DFT methods to study 1:1 complexes formed between (*R*)-NEA and 2,2,2-trifluoroacetophenone (TFAP)[14,15] and methyl-trifluoropyruvate (MTFP)[15,16] on Pt(111). In addition, methyl benzylformate (MBF)/(*R*)-NEA/Pt(111) complexes were studied by STM alone.[17] These substrates, and KPL, were chosen for study because they are representative of compounds that have been widely used to explore the Orito reaction.[18-21] The study of the TFAP/(*R*)-NEA system revealed the formation of several distinct complexes through binding of the phenyl group at specific surface sites in proximity to the ethylamine group of (*R*)-NEA. All of these complexes involved NH···O bonding. Their relative abundances and the prochiral ratios at the sub-molecular sites were determined. The study of the α-ketoester MTFP also revealed the formation of a number of distinct complexes including ones where both carbonyl groups undergo attractive interactions with (*R*)-NEA, and in which CH···O bonding in addition to NH···O bonding occurs. While KPL is also an aliphatic α-ketoester, its cyclic structure and bulky dimethyl group distinguishes it from MTFP. Furthermore, it is of direct practical interest as the (*R*)-pantolactone product is an intermediate in the synthesis of pantothenic acid, vitamin B5.[22]

Experimental Details

Ketopantolactone (purity 97%) and (*R*)-NEA (purity 99%) were purchased from Sigma-Aldrich and further purified by pumping and freeze-thaw cycles in the gas handling vacuum line prior to dosing on the surface in the ultra high vacuum (UHV) chamber at room temperature. The Pt(111) crystal, purchased from MaTecK Gmbh, was cleaned by Ar^+ (1×10^{-5} torr) bombardment at 600 K and O_2 (2×10^{-7} torr) treatment at 900 K followed by a flash annealing to 1000 K. The STM images were acquired using a SPECS Aarhus STM-150 microscope. At room temperature, the chamber was first exposed to (*R*)-NEA and then to KPL. The sample was then cooled and the reported measurements were performed at 248 K. All images were acquired at a bias voltage of 1 V on the sample and at a constant tunneling current of 0.22 nA. WSxM image treatment software was used in the adjustment of brightness and contrast.

Computational Details

All calculations were done using the GPAW software[23,24] and a grid spacing of 0.175 Å. Van der Waals interactions were taken into account by use of the optB88-vdW functional[25]. The surface was modeled by four layers of 36 Pt atoms using a self-consistent lattice constant equal to 4.02 Å. The bottom layer of the slab was fixed during relaxation. The computational unit cell is periodic in the x- and y- directions but aperiodic in the z-direction with a minimum of 6 Å of vacuum separating the atoms and the cell boundary. Complexation energies of KPL and NEA are calculated relative to the two separated molecules in the same cell to minimize effects of varying the coverage. A large number of complexes were tested using only the Γ-point. Of those, structures with a

complexation energy of 0.25 eV or greater were relaxed with 2x2 k-points until all forces were below 0.025 eV/Å.

Calculated Adsorption Geometry and Adsorption Energy of KPL on Pt(111)

We expect that the structure of modifier-substrate complexes represent a compromise between modifier-substrate interactions and the preferred adsorption configuration of the isolated molecules. The adsorption of NEA was already discussed elsewhere,[14,26] hence we only present calculations on the isolated geometry of KPL. In the most stable adsorption geometry found, the *keto*-carbonyl of KPL is bridged across two Pt atoms in an η^2-configuration, observed as an elongation of the C=O bond from 1.21 Å in the gas phase to 1.34 Å on the surface. The strong interaction is reflected in short C-Pt and O_{keto}-Pt bond lengths of 2.22 and 2.10 Å respectively. The O_{ester}-Pt bond length is 2.23 Å, however, the bond length of the ester-carbonyl is nearly unchanged relative to the gas phase value. The rest of the molecule is bent away from the surface to minimize steric repulsion between the methyl groups and the surface. The adsorption energy is calculated to be 1.25 eV on a 4x4 Pt slab, which is close to the value of 1.31 eV calculated for MTFP on Pt(111)[15] on a 6x6 Pt surface using a comparable grid spacing.

Since we have shown elsewhere[27] that residual hydrogen in the ultrahigh vacuum system can partially hydrogenate TFAP to the hydroxy intermediate on Pt(111) at room temperature, we cannot rule out that a similar process occurs for KPL to yield a half-hydrogenated adsorbate (denoted as hh-KPL). When the oxygen is hydrogenated the resulting hydroxy state will be referred to as hy-KPL, and when the carbon is hydrogenated the resulting alkoxy state will be referred to as alk-KPL. The most stable adsorption geometries found for hy-KPL and alk-KPL on Pt(111) are shown in Figure 2B and C, respectively. The principal difference between these two structures and KPL is that the atom which is hydrogenated is no longer coordinated to the surface. In the case of hy-KPL, the *keto*-oxygen lifts away from the Pt atom beneath it. The O_{keto}-Pt distance increases to 3.00 Å while the C-Pt distance decreases slightly to 2.17 Å. Hy-KPL lies in a plane that is now closer to parallel with the Pt surface. This geometry results in a structure that is 0.19 eV more stable than KPL. Conversely, for alk-KPL, the C-Pt distance increases to 3.18 Å while the O_{keto}-Pt distance decreases slightly to 2.05 Å. Alk-KPL appears more upright compared to KPL and is 0.319 eV less stable than KPL.

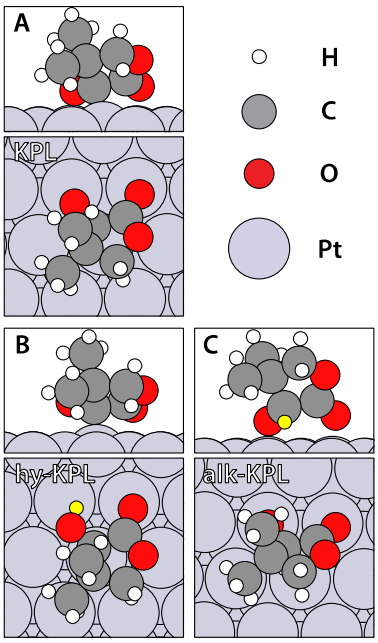

Figure 2: (A) Calculated adsorption geometry of KPL on Pt(111). (B, C) Calculated adsorption geometries, respectively, of hydroxy (hy-KPL) and alkoxy (alk-KPL) half-hydrogenated states of KPL on Pt(111). The additional hydrogen in hy-KPL and alk-KPL is highlighted in yellow.

Calculating Favourable KPL/(*R*)-NEA Complexation Geometries

As described above in Computational Details, an initial search for stable complexation structures was carried out. The results of this search are summarized in Figure 3, using a colour-bar to indicate the complexation energies. The reference for (*R*)-NEA-1 complexes is a separated non-interacting adsorbed (*R*)-NEA-1/KPL pair, while the reference for (*R*)-NEA-2 complexes is a similar separated (*R*)-NEA-2/KPL pair. Conversion between (*R*)-NEA-1 and (*R*)-NEA-2 does not occur under the experimental conditions. Thus, the difference in energy between the two conformations is not considered when calculating the complexation energy. From the scan, several stable complexes are found. For example, a particularly stable complex is calculated for (*R*)-NEA-2/pro-R KPL, with KPL located to the left-side of the ethylamine group. The designation pro-R KPL is made on the basis that hydrogen addition from the surface would lead to the (*R*)-pantolactone product. The most favourable structures were then chosen for higher-level calculations.

The resulting complexation energies for (*R*)-NEA/KPL/Pt(111) are ranked in Figure 4. Given the possibility of partial hydrogenation, another more focused search was performed using hh-KPL species. A number of the most stable KPL complexes were partially hydrogenated and relaxed. Thus, Figure 4 also includes structures formed by both hy-KPL and alk-KPL species, on a common energy scale using the same optimised

reference structures as for the non-hydrogenated species, but with a non-interacting hydrogen atom placed on the surface.

Initially, considering only KPL complexes, Figure 4 immediately provides two general insights. First, the calculated complexation energy for each of the three best (*R*)-NEA-2/KPL structures is greater than for all (*R*)-NEA-1/KPL complexes. Second, while there are several (*R*)-NEA-1/KPL complexes of similar stability, the three best (*R*)-NEA-2/KPL complexes have more widely spaced stabilization energies.

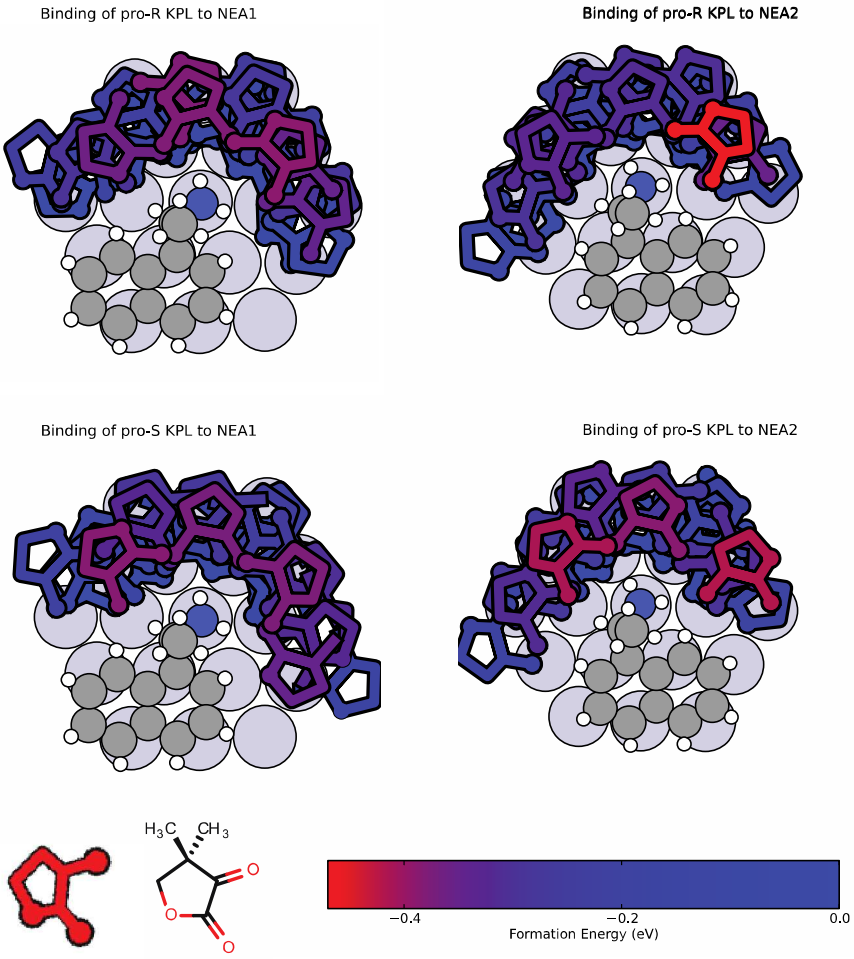

Figure 3. Exploratory DFT scan of structures for (*R*)-NEA-1/KPL and (*R*)-NEA-2/KPL complexes. Different complexes are marked by different positions of the molecular symbol explained in the bottom of the Figure. The upper panel shows pro-R KPL complexes and the lower panel shows pro-S KPL complexes. A colour-bar is provided to indicate the complexation energies, with red indicating the most stable structures found. The reference energy for (*R*)-NEA-1/KPL structures is a case where the adsorbates are separated, and the same type of convention is used to define the reference energy for (*R*)-NEA-2/KPL complexes.

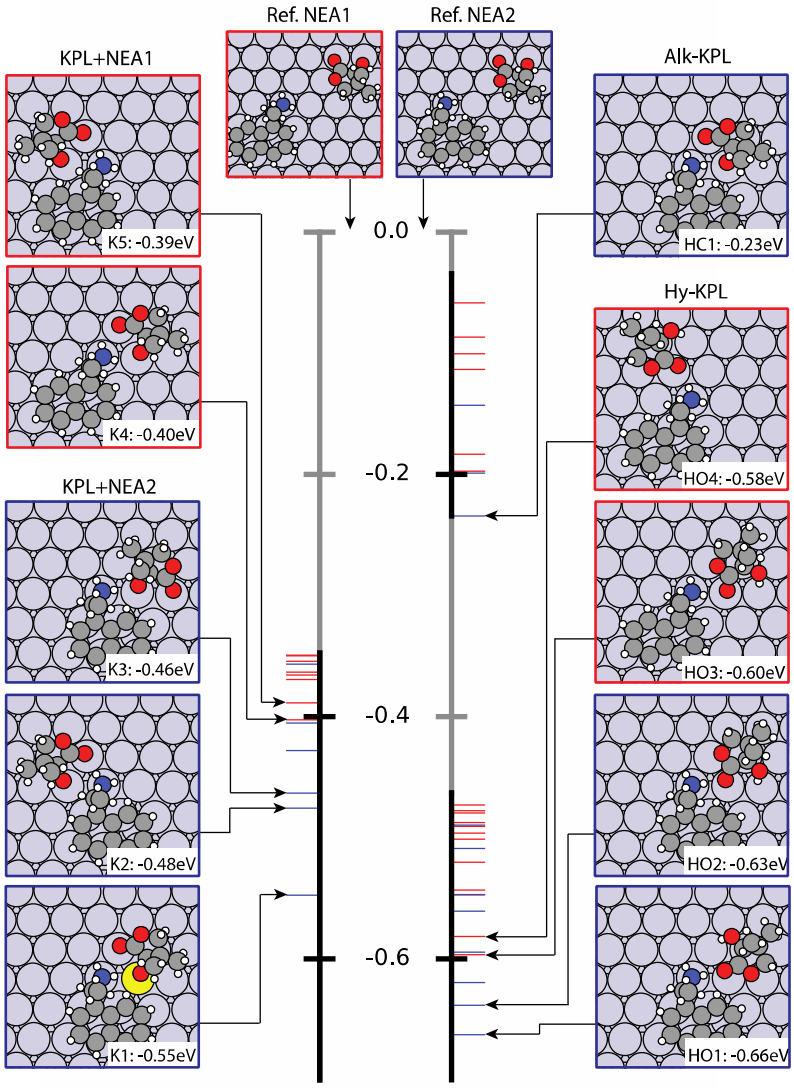

Figure 4. Energy diagram showing the most stable (*R*)-NEA/KPL complexes (left) and the most stable (*R*)-NEA/hh-KPL complexes (right), as well as non-interacting reference structures (top). Red and blue lines mark the energy of (*R*)-NEA-1 and (*R*)-NEA-2 complexes, respectively. Complexation energies falling on the grey part of the energy scale are not marked. (*R*)-NEA-1 complexes use Ref. NEA1 (top), while (*R*)-NEA-2 complexes use Ref. NEA2 (top) as their reference, respectively, to determine the complexation energy.

The three most stable DFT-predicted (*R*)-NEA-2/KPL complexes are K1, K2 and K3 (Figure 4). Each of these complexes forms an NH···O bond. In addition, each of them also forms a CH···O bond. The *keto*-carbonyl of K3 simultaneously interacts with an NH and an arene-CH bond, while occupying a bridge chemisorption site. In contrast, the

ester-carbonyl does not interact with (*R*)-NEA-2 in complex K3; it points away from the modifier, with the oxygen atom of the *ester*-carbonyl placed 2.29 Å over a Pt atom. The overall orientation imposed on KPL by this combination of chemisorption and intermolecular interaction establishes a pro-S configuration in structure K3. For K1 and K2, both the *ester*- and the *keto*-carbonyl groups are in interaction with the modifier, forming a two-carbonyl contact. In the case of K2, the *keto*-carbonyl is in interaction with the CH bond at the chiral center on (*R*)-NEA-2 while the *ester*-carbonyl separately forms an NH···O bond. As a result, a pro-S configuration is imposed on KPL, and it is located to the top-left of the ethylamine group. In contrast, K1 is in a pro-R configuration where its *keto*-carbonyl undergoes a combination of NH···O and CH···O bonding, similar to that for K3, while its *ester*-carbonyl oxygen is in proximity to the two NH bonds and 2.44 Å distant from a Pt atom.

K1 is calculated to be the most stable complex, and we attribute this to the fact that it forms *ester*-carbonyl NH···O bonding in addition to the highly favourable *keto*-carbonyl/NH···O plus arene-CH···O combination revealed by K3. The suggested participation of CH···O bonding in stereodirecting KPL, is in line with several examples of stereocontrol involving CH···O interactions in organic synthesis,[28-31] as well as with our proposal that CH···O bonding can play a stereodirecting role in the Orito reaction.[7,16,32]

The stability of complexes formed by placing KPL to the right-hand side of (*R*)-NEA-2 appears to be related to the sub-molecular pocket created by the combination of one NH···O bond plus one arene-CH···O bond plus one Pt atom. Placing the *keto*-carbonyl oxygen over this Pt atom (indicated in yellow for the K1 complex in Figure 4) permits the formation of a strong NH···O/CH···O combination as well as a η^2-chemisorption bond in which the carbonyl group is bridged between two Pt atoms. In contrast, the (*R*)-NEA-1/Pt(111) chemisorption footprint does not place a Pt atom in a position to permit simultaneous NH···O and CH···O bonding to the *keto*-carbonyl, along with carbonyl group η^2-chemisorption bonding, when KPL is located to the right-hand side of the ethylamine group. The stability of complexes where this sub-molecular pocket is present indicates the significant role that the chemisorption geometry of both the modifier and the substrate, in addition to the intermolecular interaction geometry, play in determining the relative stabilities of different complexes.

Considering now the partially hydrogenated KPL complexes in Figure 4, it is clear that hydrogenating the *keto*-oxygen is preferable to hydrogenating the *keto*-carbon. The most stable alk-KPL complex (structure HC1) is 0.43 eV less stable than the most stable hy-KPL complex (structure HO1). Based on this result, we only consider further complexes formed by hy-KPL. We find that the best hy-KPL complexes are more stable than the best complexes formed by KPL. This would appear to arise from a strong *ester*

carbonyl interaction with the amine group. It is presumed that since the *keto*-oxygen is no longer coordinated to the surface, the $NH^{\cdots}O_{ester}$ hydrogen bond geometry can be better optimized in order to maximize its strength.

STM measurements of (*R*)-NEA/KPL complexes

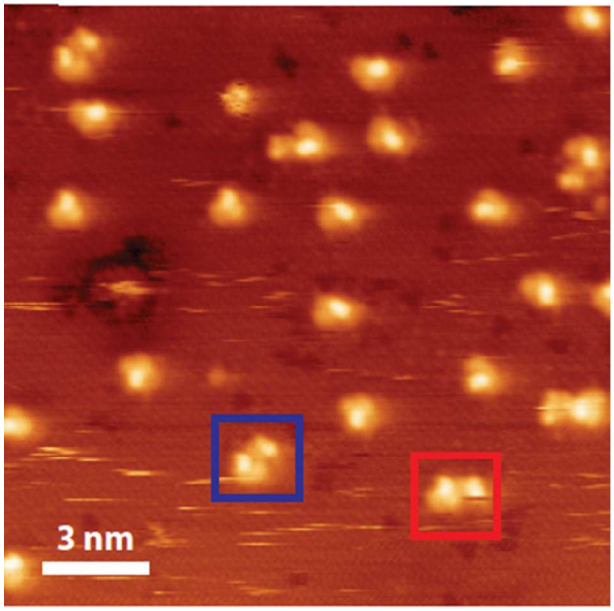

Figure 5. Large-scale STM image of KPL and (*R*)-NEA on the Pt(111) surface at 248 K. The blue and red squares mark KPL/(*R*)-NEA-2 and KPL/(*R*)-NEA-1 bimolecular complexes, respectively

Only the lower STM temperature data are presented, since they display the best molecular resolution and the best atomic resolution of the metal surface. A large scan image is shown in Figure 5. In this experiment, roughly one quarter of the (*R*)-NEA molecules are in complexes, and essentially all of the complexes are bimolecular (so-called 1:1 complexes). At higher KPL to (*R*)-NEA surface coverage ratios, $(KPL)_2$/(*R*)-NEA complexes are also frequently observed. Under all conditions, almost all of the complexes are formed with KPL located in proximity to the bright protrusion of the (*R*)-NEA motifs: that is, with KPL located in proximity to the ethylamine group. This binding configuration offers the possibility of forming $NH^{\cdots}O$ bonds. In this context, it should be noted that recent *in situ*[33] and *operando*[18] studies by Baiker and co-workers reveal $NH^{\cdots}O$ bonding between KPL and cinchonidine on supported Pt catalysts.

A visual inspection of Figure 5 reveals that several different complexation configurations are formed. By referring back to the DFT calculated complexes, we now wish to define the precise combination of KPL adsorption geometry and KPL/(*R*)-NEA intermolecular interaction leading to specific complexation structures. To do so, we first need to carefully categorize and describe the information contained in the large set of STM data. As a first step, we qualitatively describe the images of isolated and complexed

KPL, and we schematically summarize the distribution of complexes. Figure 6 displays an image (A) of isolated KPL acquired at 215 K and an image (B, C) of a (*R*)-NEA/KPL complex acquired at 248 K. Three protrusions are sufficient to give a description of isolated KPL and of KPL in all complexes, an example of which is shown in Figure 6C. The protrusion labeled 1 is the brightest. The protrusion labeled 2 is smaller and less bright. The protrusion labeled 3 is dimmer than 1 or 2. In all of the complexes, the protrusion 3 points towards (*R*)-NEA. Two adsorption states of (*R*)-NEA need to be specified, since it occupies two stable rotameric states on Pt(111). As described in detail in previous publications,[14,26] these states are labeled (*R*)-NEA-1 and (*R*)-NEA-2, and both form a naphthyl π-bond and an N-Pt bond to the surface. Their calculated structures are included in Figures 3 and 4, and their STM images are clearly distinguishable as shown by the two selected examples in Figure 5. Figure 6 B, C shows an (*R*)-NEA-2/KPL complex.

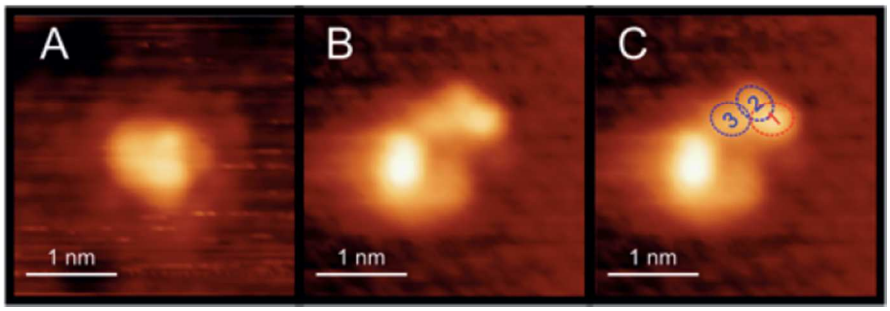

Figure 6. STM images of (A) an isolated KPL molecule on Pt(111) at 215 K and (B, C) an (*R*)-NEA-2/KPL complex on Pt(111) at 248 K. KPL in all of the observed complexes show the three protrusions labeled in (C).

In order to systematically characterize the geometry of the (*R*)-NEA/KPL complexes, STM images were overlaid with masks as described by Groves et al.[15] Once all the complexes had been covered, the original STM image was removed leaving only the masks. This was saved as a vector graphics file, which enabled a facile extraction of geometry coordinates between the modifier and the KPL. (*R*)-NEA is approximated by two ellipses, one large one and one small, which are interpreted as the naphthyl and ethylamine groups respectively. Each KPL is represented by three ellipses, one for each protrusion, as described in the previous paragraph.

Figure 7 is a schematic illustration of the observed distribution of complexes around (*R*)-NEA-1 (A) and (*R*)-NEA-2 (B). The crosses qualitatively locate protrusion 3 of KPL with respect to (*R*)-NEA and the resulting clusters of data points serve to illustrate, without molecular detail, the range of binding sites observed. In order to extract the molecular details required to specify the precise binding configurations, we now turn to a quantitative description of the data.

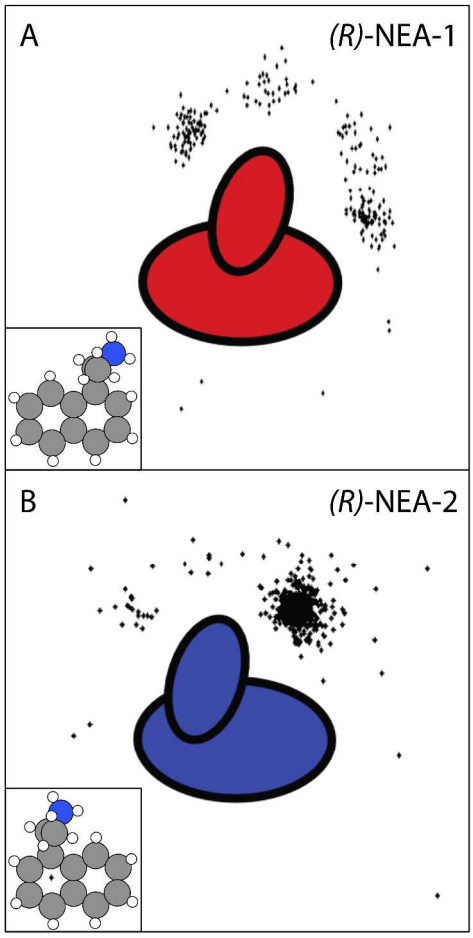

Figure 7. Schematic illustration of the occupation of different binding sites around (*R*)-NEA-1 (red) and (*R*)-NEA-2 (blue) in a population of 1:1 complexes. Each cross schematically represents a data point for one complex, giving the rough location of KPL with respect to (*R*)-NEA. The large ellipses represent the naphthyl groups and the smaller ellipses represent the ethylamine groups.

The STM images are categorized according to the θ,φ notation (Figure 8) introduced by Groves et al.,[15] where θ describes the position of the substrate around a chemisorbed (*R*)-NEA molecule, and φ describes the directionality or orientation of the substrate at that position. In this case, protrusion 1 is used to define θ_{STM}, while a line through protrusion 2 is used to define φ_{STM}, as illustrated in Figure 8. This procedure is carried out for large sets of data, resulting in clusters of points (each point representing one complex) on the $(\theta\text{-}\varphi)_{STM}$ scatter plot. In parallel, $(\theta\text{-}\varphi)_{DFT}$ scatter plots are constructed from the set of most stable calculated DFT structures. The match between the $(\theta\text{-}\varphi)_{DFT}$ and $(\theta\text{-}\varphi)_{STM}$ plots is used to assign the complexation structures giving rise to the most abundant STM images. This procedure evidently requires knowledge of how the STM images of KPL relate to the molecular structure of KPL.

In order to determine the relation between STM images of KPL and its structure, STM simulations of the K1 and HO2 complexes from Figure 4 were calculated. They are shown in Figure 9A and B, respectively, and include the positions of all the atoms. For the KI complex simulation (9A), the two methyl groups are represented by a bright protrusion, the CH_2 group is represented by a second dimmer protrusion, and the ester carbonyl by a third dim protrusion. Based on the simulated image, we use, as shown in Figure 8A, the point equidistant between the two carbons of the methyl groups to define θ_{DFT}. Similarly, we use a line through the carbon in the CH_2 group to define φ_{DFT}.

The (*R*)-NEA-2/hy-KPL complex HO2 was selected for image simulation as it is one of the two most stable hydroxy complexes, and as for K1 it is a pro-R configuration. This choice is made so that the differences between the simulated images of K1 and HO2 can be more reliably attributed to partial hydrogenation instead of any other factor. As was already seen from the calculated structure shown in Figure 2B, upon partial hydrogenation, hy-KPL lies more horizontally on the surface compared to KPL. This results in one of the two methyl groups being much further above the other. This is captured in the simulated STM image by the bright protrusion becoming more intense, relative to the K1 simulation. As a result, for hydroxy species, θ_{DFT} will be defined by the position that is one quarter the distance between the high methyl carbon and the low methyl carbon. The second dimmer protrusion is still expected to be centered on the CH_2 group. Thus, the CH_2 carbon will also be used to define φ_{DFT} values for complexes formed by hy-KPL.

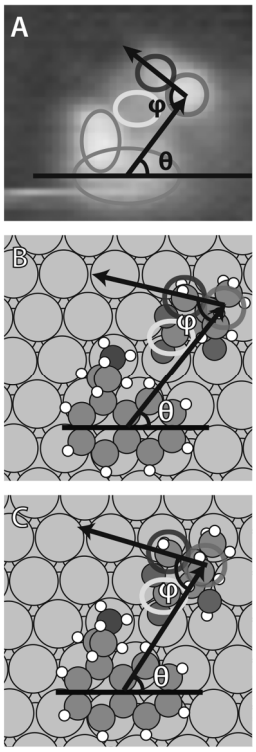

Figure 8. Definition of the θ,φ parameters used to quantify (A) the STM data for (*R*)-NEA/KPL complexes and (B, C) the DFT data for (*R*)-NEA/KPL and (*R*)-NEA/hy-KPL complexes.

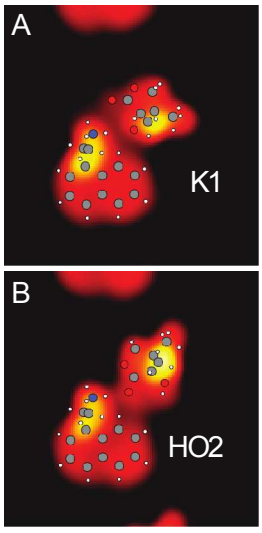

Figure 9. DFT simulated STM images (A and B) of the (*R*)-NEA-2/KPL and (*R*)-NEA-2/hy-KPL complexes labeled as K1 and HO2, respectively, in Figure 4.

Two (θ-φ) plots are required, one for (*R*)-NEA-1 and one for (*R*)-NEA-2. These two scatter plots are presented in Figure 10. They immediately show that (*R*)-NEA-1 and (*R*)-NEA-2 display different complexation patterns towards KPL. Since the two conformers present distinct spatial arrangements of functional groups to an incoming prochiral substrate, they effectively behave as two different chiral modifiers. The difference can be seen both in terms of the relative number of complexes formed and in their preference for specific complexation geometries. For low KPL to (*R*)-NEA ratios, where the complexes are almost exclusively 1:1 structures and approximately one quarter of the (*R*)-NEA molecules are in complexes, (*R*)-NEA-2 out-competes (*R*)-NEA-1 in that it forms the majority (approximately two thirds) of complexes despite the fact that it is the minority (approximately one third) chiral species present on the surface. This result is in agreement with the DFT calculations: the most stable (*R*)-NEA-2/KPL complexes are significantly more stable than the most stable (*R*)-NEA-1/KPL complexes. In contrast, for experiments where the KPL to NEA ratio is high, (*R*)-NEA-1 complexes become the most abundant, but under these conditions there is a significant proportion of termolecular complexes (data not shown).

The two modifier conformations also differ in that (*R*)-NEA-2 is more selective in its interaction with KPL, in the sense that data points for (*R*)-NEA-2/KPL are clustered into a smaller number of groups. This selectivity is made most apparent by the histogram representation of the data in the upper panel of Figure 10, and may already be appreciated from Figure 7. In contrast the (*R*)-NEA-1/KPL complexes show a more evenly spread range of structures. Again, this result is in agreement with the DFT calculations where it was found that there was a significant separation in energy between the most favourable (*R*)-NEA-2/KPL complexes, while this separation is far less pronounced with the (*R*)-NEA-1/KPL complexes.

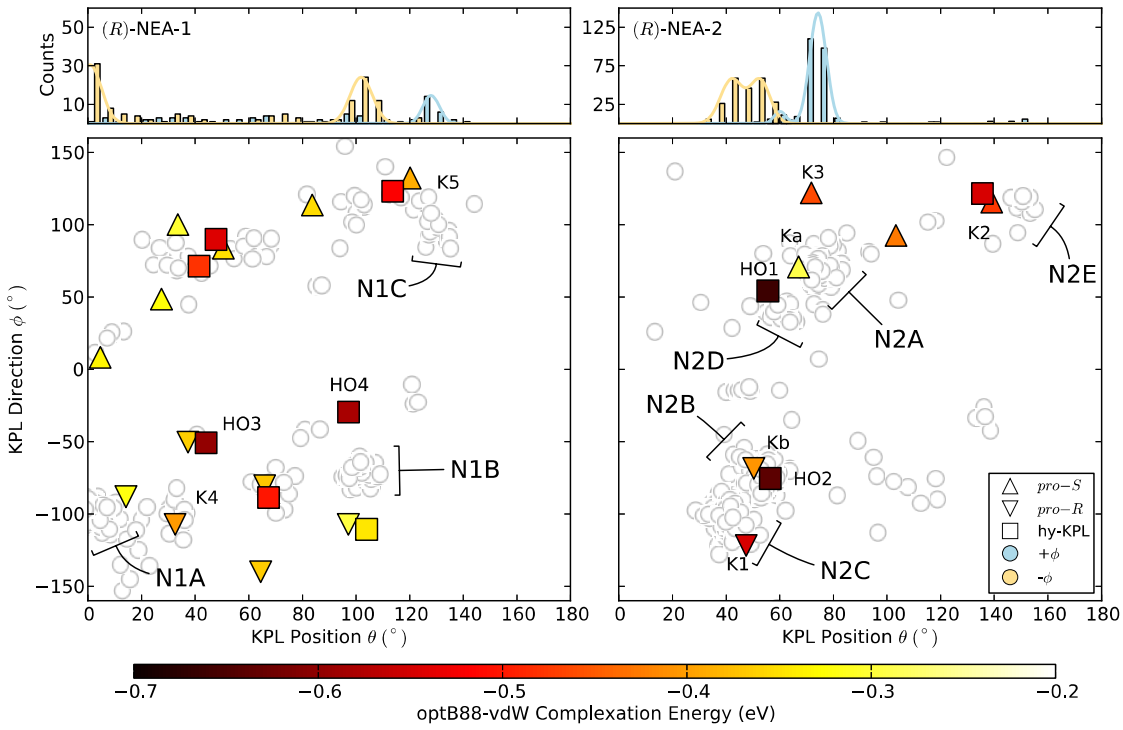

Figure 10. Scatter-plots (θ,φ) for 1:1 (*R*)-NEA/KPL complexes. Each circle represents a single complex. As indicated in the insert, the circles are coloured blue and orange depending on the sign of the φ value. The populations of complexes are shown in histogram form in the top panel. The triangles refer to (θ,φ) values for DFT calculated most stable complexes. Upwards pointing triangles indicate pro-S structures while downwards pointing triangles indicate pro-R structures. The squares refer to the (*R*)-NEA/hy-KPL complexes shown in Figure 4. The notation N1A-N1C and N2A-N2E is used to specify the clusters of data containing the specific STM images shown in Figure 11. The notation Ka and Kb refer to the less stable calculated complexes shown in Figure 12.

The match between the $(\theta\text{-}\varphi)_{STM}$ to the $(\theta\text{-}\varphi)_{DFT}$ representations of the entire set of (*R*)-NEA-1 and (*R*)-NEA-2 data is not sufficiently good to reliably assign all observed STM data clusters. However, assuming that Figure 10 represents the best fit between the STM and DFT data, we assign molecular structures to the most abundant (*R*)-NEA complexes shown in Figure 11. The five STM images N2A-N2E shown in Figure 11 come, respectively, from data points within the clusters labeled N2A-N2E in Figure 10. Considering only the formation of (*R*)-NEA-2/KPL complexes, and comparing to the most stable calculated complexes, leads to an assignment of the N2C, N2A and N2E clusters to K1, K3 and K2, respectively, the structures of which are shown in Figure 4. However, it can be seen from Figure 10 that a considerably less stable calculated complex (Ka) actually provides a better match to the N2A cluster. Structure Ka, shown in

Figure 12, is the pro-S complex formed by inverting KPL relative to its orientation in K1, so that the *ester*-carbonyl interacts at N-H/C-H and the *keto*-carbonyl interacts with the amine group. Similarly, the Kb complex shown in Figure 12 provides the best match to cluster N2B, despite the fact that it is not among the most stable calculated complexes. A better fit to cluster N2B, involving a very stable complex, is found if we also consider (*R*)-NEA-2/hy-KPL complexes. In the latter interpretation, cluster N2B is assigned to the hydroxy complex H02. Along the same lines, the cluster N2D is most readily assigned to the hydroxy complex H01. From Figure 4, it can be seen that K1 can be converted to HO2 by adding a proton to the *keto*-oxygen and then rotating the resulting hydroxy intermediate until the *ester*-carbonyl forms a combined NH···O/CH···O interaction. Similarly K3 can be converted to HO1 by forming the hydroxy intermediate and rotating around the resulting Pt-C bond until the ester group is captured by NH···O/CH···O interactions. This description is not meant to imply that we have dynamical information, but rather to illustrate that an intuitive relation can be made between K1 and HO2 and between K3 and HO1.

It can be seen that that there is poor prochiral selection of KPL by (*R*)-NEA-2, with roughly equal abundances of pro-R and pro-S complexes. This is in contrast to what was observed for (*R*)-NEA-2/MTFP, where very strong prochiral selectivity was observed, involving a two-carbonyl interaction leading to the preferential formation of a complex analogous to the K1 complex found for KPL. Further work is underway to better understand the different behavior of MTFP and KPL towards complexation to (*R*)-NEA on Pt(111). The overall prochiral ratio observed for KPL/(*R*)-NEA on Pt(111) is much less than the 76:24 *R* to *S* enenantiomeric ratio observed[9] in hydrogenation of the KPL on (*R*)-NEA modified Pt (Figure 1). This discrepancy could arise from a number of factors, including protonation of (*R*)-NEA on the Pt catalyst or though kinetic control where the rate of hydrogenation in pro-R complexes such as K1 is fastest.

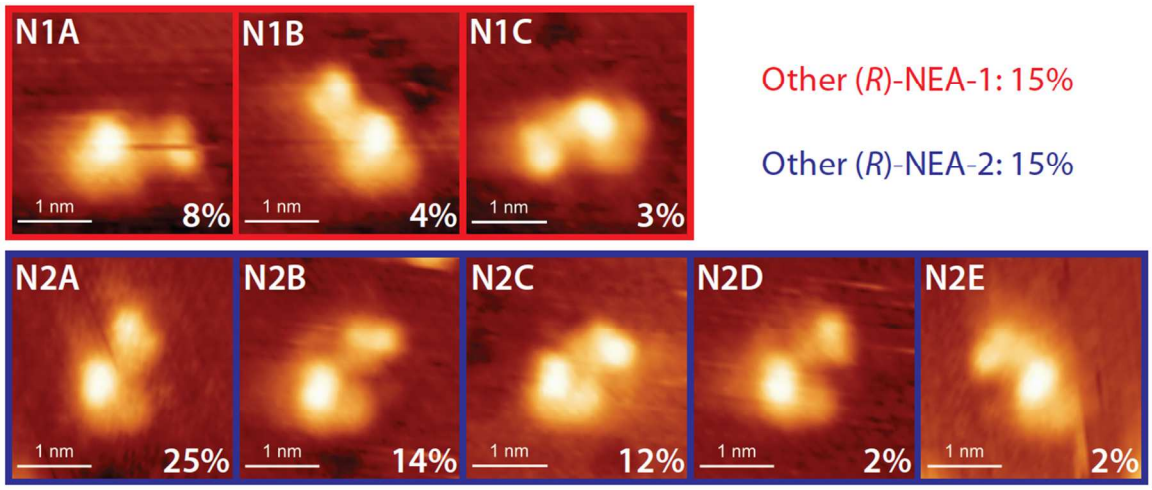

Figure 11. STM images representative of abundant (*R*)-NEA/KPL complexes formed on Pt(111) at 248 K. The top panel shows (*R*)-NEA-1/KPL complexes. The bottom panels show (*R*)-NEA-2/KPL complexes. The relative abundance of each of the imaged motifs is given low KPL to (*R*)-NEA ratio data is characteristic of a sample of exclusively 1:1 complexes. A variety of additional types of motifs are observed and their combined abundance is labeled under the headings Other (*R*)-NEA-1 and Other (*R*)-NEA-2.

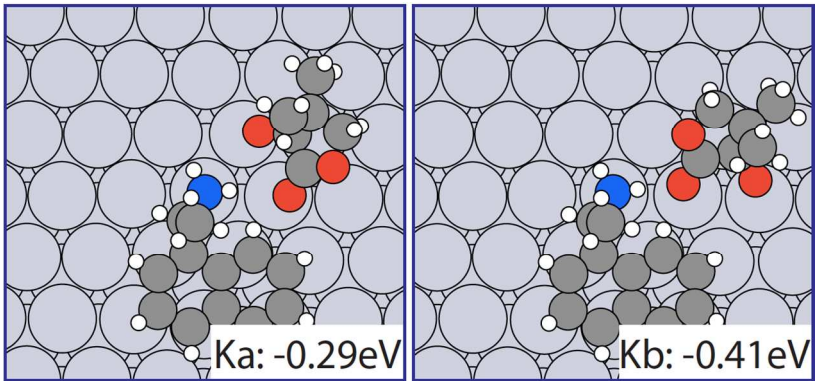

Figure 12. Structures and complexation energies of the calculated Ka and Kb (*R*)-NEA-2/KPL complexes noted in Figure 10. These complexes are not shown in Figure 4 as they are not among the most stable structures found.

The preference for the formation of (*R*)-NEA-2/KPL complexes shown by both the experimental and calculated data is interesting in terms of the phenomenon of substrate induced conformation change in chiral modifiers on Pt catalysts reported by Baiker and co-workers.[34,35] They monitored the stereochemistry of the slow hydrogenation of the quinolone group of cinchonidine during the asymmetric hydrogenation of ethyl pyruvate, methyl benzylformate (MBF) and KPL. Their experiment provided a measurement of the relative surface coverage of cinchonidine

conformations that differ in terms of which face of the quinolone group is turned toward the surface. For each of the three α-ketoester substrates, they found that the substrate induced a significant change in the ratio of adsorption conformations of cinchonidine. These changes were observed in solution under true reaction conditions. Our experiments are carried out under ultrahigh vacuum conditions in the absence of solvent and using (*R*)-NEA rather than cinchonidine. The calculated difference in adsorption energy between (*R*)-NEA-2 and (*R*)-NEA-1 on Pt(111) is 0.14 eV in favour of (*R*)-NEA-1. From Figure 9, it can be seen that the calculated complexation energy for (*R*)-NEA-2 can balance out or exceed this difference. This suggests that in the presence of a solvent where an adsorption equilibrium operates, KPL would cause the proportion of adsorbed (*R*)-NEA-2 to increase. Specifically, we would attribute such an effect to the ability of (*R*)-NEA-2 to form complexes such as K1 where multiple optimal non-covalent interactions are allowed.

Conclusions

A combination of van der Waals corrected DFT calculations and STM measurements were used to determine the structure and stability of bimolecular complexes formed between ketopantolane (KPL) and (*R*)-1-(1-naphthyl)ethylamine on Pt(111). The ultimate objective of such studies is to gain a better understanding of how chirality transfer occurs in hydrogenation reactions on chirally modified metal surfaces. The system under study is of particular interest, since the (*R*)-NEA is known to be a reasonably effective chiral modifier for the asymmetric hydrogenation of KPL on supported platinum catalysts.[9]

Two conformers of the chiral molecule, (*R*)-NEA-1 and (*R*)-NEA-2, are present on the Pt(111) surface and they interact in distinct ways with KPL. The STM results show that (*R*)-NEA-2/KPL complexes are more abundant despite the fact that (*R*)-NEA-1 is the majority conformer. The STM data also show that (*R*)-NEA-2 forms a smaller set of complexes than (*R*)-NEA-1; that is, it captures KPL in a smaller number of binding sites. Both of these experimental observations are reflected in the calculated data: (*R*)-NEA-2/KPL complexes show higher complexation energies, and the energies for different (*R*)-NEA-1/KPL structures are more closely spaced. The most stable calculated (*R*)-NEA-2/KPL complex displays multiple non-covalent intermolecular bonding. Both carbonyl groups form NH···O bonds to the modifier, and the *keto*-carbonyl group also forms an arene-CH···O interaction. In this particular complex, the oxygen of the *keto*-carbonyl forms a bond to a Pt atom located in a position where the oxygen can simultaneously form NH···O and CH···O bonds and participate in an η^2-(C,O) chemisorption interaction. This precise two-carbonyl contact arrangement, which stereodirects KPL into a pro-R configuration and activates the carbonyl group, is an

example of how the chemisorption geometries of both the modifier and the substrate, the atomic structure of the metal and multiple non-covalent interactions combine to define a chiral pocket.

It is necessary to invoke the presence of both KPL and partially hydrogenated (hydroxy) hy-KPL in order to match the best DFT calculated structures to the relative abundances of complexes, and to the clusters of STM motifs seen in the experimental data. The partially hydrogenated KPL is attributed to the presence of residual hydrogen in the UHV system. We relate stable KPL complexes to stable hy-KPL complexes through rotation on the surface to replace a *keto*-carbonyl/modifier interaction with an *ester*-carbonyl/modifier interaction.

The overall pro-R:pro-S prochiral ratio observed for the surface complexes is much less than the *R*:*S* enatiomeric ratio reported by Baiker and co-workers[9] for the hydrogenation of KPL on (*R*)-NEA modified Pt/Al_2O_3 in acetic acid. Further studies are underway to investigate this effect.

Acknowledgements

Financial support from the The Danish Council for Independent Research Nature and Universe and the Lundbeck Foundation is gratefully acknowledged. The work was also supported by NSERC, FQR-NT and the CFI grants. The STM work was carried out within the FQRNT funded Center on Catalysis and Green Chemistry (CCVC). Y.D. and J.-C. L. acknowledge NSERC and FQRNT graduate student scholarships, respectively.

References

1. T. Bürgi and A. Baiker, *Acc. Chem. Res.*, 2004, **37**, 909–17.

2. T. Mallat, E. Orglmeister, and A. Baiker, *Chem. Rev.*, 2007, **107**, 4863–90.

3. G. Kyriakou, S. K. Beaumont, and R. M. Lambert, *Langmuir*, 2011, **27**, 9687–95.

4. H.-U. Blaser and M. Studer, *Acc. Chem. Res.*, 2007, **40**, 1348–56.

5. A. G. Trant and C. J. Baddeley, *J. Phys. Chem. C*, 2011, **115**, 1025–1030.

6. D. Y. Murzin, P. Mäki□Arvela, E. Toukoniitty, and T. Salmi, *Catal. Rev.*, 2005, **47**, 175–256.

7. S. Lavoie, M.-A. Laliberté, I. Temprano, and P. H. McBreen, *J. Am. Chem. Soc.*, 2006, **128**, 7588–93.

8. Y. Orito, S. Imai, S. Niwa, and G.-H. Nguyen, *J. Synth. Org. Chem. Jpn.*, 1979, **37**, 173–174.

9. E. Orglmeister, T. Mallat, and A. Baiker, *Adv. Synth. Catal.*, 2005, **347**, 78–86.

10. E. Tálas and J. L. Margitfalvi, *Chirality*, 2010, **22**, 3–15.

11. A. D. Gordon and F. Zaera, *Angew. Chem. Int. Ed. Engl.*, 2013, **52**, 3453–6.

12. L. Burkholder, M. Garvey, M. Weinert, and W. T. Tysoe, *J. Phys. Chem. C*, 2011, **115**, 8790–8797.

13. E. Schmidt, A. Vargas, T. Mallat, and A. Baiker, *J. Am. Chem. Soc.*, 2009, **131**, 12358–67.

14. V. Demers-Carpentier, G. Goubert, F. Masini, R. Lafleur-Lambert, Y. Dong, S. Lavoie, G. Mahieu, J. Boukouvalas, H. Gao, A. M. H. Rasmussen, L. Ferrighi, Y. Pan, B. Hammer, and P. H. McBreen, *Science*, 2011, **334**, 776–80.

15. M. N. Groves, G. Goubert, A. M. H. Rasmussen, Y. Dong, J.-C. Lemay, V. Demers-Carpentier, P. H. McBreen, and B. Hammer, *Surf. Sci.*, 2014, DOI: 10.1016/j.susc.2014.03.008.

16. V. Demers-Carpentier, A. M. H. Rasmussen, G. Goubert, L. Ferrighi, Y. Dong, J.-C. Lemay, F. Masini, Y. Zeng, B. Hammer, and P. H. McBreen, *J. Am. Chem. Soc.*, 2013, **135**, 9999–10002.

17. G. Goubert and P. H. McBreen, *ACS Catal.*, 2014, **4**, 847–854.

18. F. Meemken, K. Hungerbühler, and A. Baiker, *Angew. Chem. Int. Ed. Engl.*, 2014, **53**, 8640-4.

19. G. Martin, P. Mäki-Arvela, D. Y. Murzin, and T. Salmi, *Catal. Sci. Technol.*, 2014, **4**, 170-8.

20. G. Szőllősi, K. Balázsik, I. Bucsi, T. Bartók, and M. Bartók, *Catal. Commun.*, 2013, **32**, 81–85.

21. N. V Rees, R. J. Taylor, Y. X. Jiang, I. R. Morgan, D. W. Knight, and G. A. Attard, *J. Phys. Chem. C*, 2011, **115**, 1163–1170.

22. D. J. Ager, A. H. M. de Vries, and J. G. de Vries, *Chem. Soc. Rev.*, 2012, **41**, 3340–80.

23 J. J. Mortensen, L. B. Hansen, and K. W. Jacobsen, *Phys. Rev. B,* 2005, ***71,*** *035109*.

24 J. Enkovaara, C. Rostgaard, J. J. Mortensen, J. Chen, M Dułak, L. Ferrighi, J. Gavnholt, C. Glinsvad, V. Haikola, H. A. Hansen, H. H. Kristoffersen, M. Kuisma, A. H. Larsen, L. Lehtovaara, M. Ljungberg, O. Lopez-Acevedo, P. G. Moses, J. Ojanen, T. Olsen, V. Petzold, N. A. Romero, J. Stausholm-Møller, M. Strange, G. A. Tritsaris, M. Vanin, M. Walter, B. Hammer, H. Häkkinen, G. K. H. Madsen, R. M. Nieminen, J. K. Nørskov, M. Puska, T. T. Rantala, J. Schiøtz, K. S. Thygesen, K. W. Jacobsen, *J. Phys.: Condens. Matter* 2010, ***22,*** 253202.

25 J, Klimeš, D. R. Bowler, and A. Michaelides, J. Phys.: Condens. Matter 2010, 22, 022201

26. G. Goubert, A. M. H. Rasmussen, Y. Dong, M. N. Groves, P. H. McBreen, and B. Hammer, *Surf. Sci.*, 2014, DOI: 10.1016/j.susc.2014.03.021

27. G. Goubert, M. N. Groves, Y. Dong, J.-C. Lemay, P. H. McBreen, and B. Hammer, *Submitt. Publ.*

28. R. C. Johnston and P. H.-Y. Cheong, *Org. Biomol. Chem.*, 2013, **11**, 5057–64.

29. E. J. Corey and T. W. Lee, *Chem. Commun.*, 2001, 1321–1329.

30. P. Maity, R. P. Pemberton, D. J. Tantillo, and U. K. Tambar, *J. Am. Chem. Soc.*, 2013, **135**, 16380–3.

31. Z. Huang, L. H. Lim, Z. Chen, Y. Li, F. Zhou, H. Su, and J. S. Zhou, *Angew. Chem. Int. Ed. Engl.*, 2013, **52**, 4906–11.

32. V. Demers-Carpentier, Y. Pan, G. Mahieu, G. Goubert, B. Hammer, and P. H. McBreen, *J. Phys. Chem. C*, 2011, 1355–1360.

33. F. Meemken, N. Maeda, K. Hungerbühler, and A. Baiker, *Angew. Chem. Int. Ed. Engl.*, 2012, **51**, 8212–6.

34. Z. Cakl, S. Reimann, E. Schmidt, A. Moreno, T. Mallat, and A. Baiker, *J. Catal.*, 2011, **280**, 104–115.

35. E. Schmidt, T. Mallat, and A. Baiker, *J. Catal.*, 2010, **272**, 140–150.